Published in final edited form as:
Neuroimage. 2012 May 15; 61(1): 115–130. doi:10.1016/j.neuroimage.2012.02.059.

Enhancement of Temporal Resolution and BOLD Sensitivity in Real-Time fMRI using Multi-Slab Echo-Volumar Imaging

Stefan Posse[1,2,3], **Elena Ackley**[1], **Radu Mutihac**[1,4,5], **Jochen Rick**[6], **Matthew Shane**[7], **Cristina Murray-Krezan**[8], **Maxim Zaitsev**[6], and **Oliver Speck**[9]

[1]Department of Neurology, University of New Mexico School of Medicine, Albuquerque, NM, USA

[2]Department of Electrical and Computer Engineering, University of New Mexico, Albuquerque, NM, USA

[3]Department of Physics and Astronomy, University of New Mexico, Albuquerque, NM, USA

[4]Department of Physics, University of Bucharest, Bucharest, Romania

[5]Division of Psychiatry and Neuroscience, Walter Reed Army Institute of Research, Silver Spring, MD, USA

[6]Department of Radiology, Medical Physics, University Medical Center Freiburg, Freiburg, Germany

[7]The MIND Research Network, Albuquerque, NM, USA

[8]Division of Epidemiology and Biostatistics, & Preventive Medicine, Department of Internal Medicine, University of New Mexico Health Sciences Center, Albuquerque, NM, USA

[9]Department of Biomedical Magnetic Resonance, Otto-von-Guericke-University Magdeburg, Magdeburg, Germany

Abstract

In this study, a new approach to high-speed fMRI using multi-slab echo-volumar imaging (EVI) is developed that minimizes geometrical image distortion and spatial blurring, and enables nonaliased sampling of physiological signal fluctuation to increase BOLD sensitivity compared to conventional echo-planar imaging (EPI). Real-time fMRI using whole brain 4-slab EVI with 286 ms temporal resolution (4 mm isotropic voxel size) and partial brain 2-slab EVI with 136 ms temporal resolution (4×4×6 mm^3 voxel size) was performed on a clinical 3 Tesla MRI scanner equipped with 12-channel head coil. Four-slab EVI of visual and motor tasks significantly increased mean (visual: 96%, motor: 66%) and maximum t-score (visual: 263%, motor: 124%) and mean (visual: 59%, motor: 131%) and maximum (visual: 29%, motor: 67%) BOLD signal amplitude compared with EPI. Time domain moving average filtering (2 s width) to suppress physiological noise from cardiac and respiratory fluctuations further improved mean (visual: 196%, motor: 140%) and maximum (visual: 384%, motor: 200%) t-scores and increased extents of activation (visual: 73%, motor: 70%) compared to EPI. Similar sensitivity enhancement, which is attributed to high sampling rate at only moderately reduced temporal signal-to-noise ratio (mean:

Corresponding author: Stefan Posse, PhD, Dept. of Neurology, The University of New Mexico School of Medicine, 1 University of New Mexico, MSC 105620, Albuquerque, NM, 87131, USA., address: sposse@unm.edu.

− 52%) and longer sampling of the BOLD effect in the echo-time domain compared to EPI, was measured in auditory cortex. Two-slab EVI further improved temporal resolution for measuring task-related activation and enabled mapping of five major resting state networks (RSNs) in individual subjects in 5 min scans. The bilateral sensorimotor, the default mode and the occipital RSNs were detectable in time frames as short as 75 s. In conclusion, the high sampling rate of real-time multi-slab EVI significantly improves sensitivity for studying the temporal dynamics of hemodynamic responses and for characterizing functional networks at high field strength in short measurement times.

Keywords

fMRI; echo-volumar imaging; real-time; temporal resolution; BOLD sensitivity; physiological noise; event related; resting state networks

INTRODUCTION

Echo-planar imaging (EPI) using blood oxygenation level-dependent (BOLD) contrast is widely used for functional magnetic resonance imaging (fMRI) in neuroscience and clinical research applications. Although EPI is capable of sampling the time course of the hemodynamic response with a standard temporal resolution of 2–3 seconds for whole brain mapping and with correspondingly faster temporal resolution for partial brain coverage, there is increased interest in achieving order of magnitude faster sampling rates for whole brain mapping to resolve heartbeat-related physiological signal fluctuation to increase sensitivity in event-related fMRI, to reduce sensitivity to intra-scan head movement and to measure regional onset differences of the hemodynamic responses without resorting to jittering the task paradigm. Recent developments of high-speed fMRI include single-shot echo-volumar imaging (EVI) (van der Zwaag et al 2006, Rabrait et al 2008, Witzel et al 2008), Inverse Imaging (InI) (Lin et al 2006, Lin et al 2008, Lin et al 2010), highly undersampled projection imaging (PI) (Grotz et al 2009) and more recently multiplexed EPI (Feinberg et al 2010) and fast volumetric imaging based on single-shot 3D rosette trajectories (Zahneisen et al 2011), all of which enable temporal resolution on the order of 100 ms or less. A recent study by Lin et al using InI demonstrated considerable improvements in hemodynamic response estimation using a moving average filter to suppress physiological noise (Lin et al 2011).

Echo-volumar imaging (EVI), one of the first 3D single-shot imaging techniques, was included in the first description of EPI and realized by Mansfield and colleagues a decade later (Mansfield and Maudsley 1976, Mansfield et al 1977, Mansfield et al 1994). The method has been challenged by the inability of whole body gradient systems to encode 3D k-space sufficiently rapidly, resulting in geometrical image distortion, signal dropouts and spatially-varying blurring of the point spread function due to magnetic field inhomogeneity and transverse signal relaxation. Using the improved gradient performance afforded by a dedicated head gradient system Song and colleagues were able to demonstrate EVI with a 64×32×7 matrix and 3.8 mm × 6.3 mm × 5 mm spatial resolution with a readout duration of 70ms (Song et al 1994). Using local excitation to achieve partial brain coverage Yang demonstrated a 64×64×10 matrix with 3.75 mm × 5 mm x 5 mm voxel size (Yang et al 1997). After this initial phase of feasibility studies in the 1990s using 1.5 T scanners there has been renewed interest in recent years. Van der Zwaag introduced an improved version of EVI using reduced field of view (FOV) encoding, outer volume suppression and a surface coil at 3 Tesla (van der Zwaag et al 2006). Integration of parallel imaging has led to considerable improvement in image quality as demonstrated in several recent studies (Rabrait et al 2008, Witzel et al 2008, Witzel et al 2011) and proof-of-concept at 7 Tesla

(van der Zwaag et al 2009). A variant of EVI using a square spiral with 14×14×14 spatial matrix and 14 mm voxel dimensions enabled detection of the negative dip across the brain with 100 ms temporal resolution (Lindquist et al 2008).

Although increasing the temporal resolution of fMRI is the principal goal, the increased efficiency (SNR per unit time) of 3D versus 2D encoding (Edelstein et al 1986, Hu and Glover 2007) makes EVI attractive. EVI is also considerably less sensitive to physiological noise than segmented 3D EPI methods (Poser et al 2010), which are affected by signal fluctuations between segments that lead to ghosting and increase apparent physiological signal fluctuation. Despite the technical advances, the need for specialized hardware, persistent image quality constraints due to geometrical image distortion, blurring and signal drop outs that are exacerbated by head movement, and signal drifts due to gradient instability and steady-state effects remain considerable challenges for routine applications, in particular at high magnetic field strength. Practical applications of EVI are also hampered by time-consuming image reconstruction of large amounts of data generated by EVI, and real-time fMRI with EVI has yet to be demonstrated.

In this study we developed a new approach to whole brain EVI using multi-slab excitation and single-shot 3D encoding with GRAPPA partial parallel imaging (Griswold et al 2002) within each slab to strongly reduce geometrical distortion and blurring while only moderately reducing temporal resolution compared to single-shot EVI. We demonstrate temporal resolution of 286 ms for whole brain acquisition (4 mm isotropic voxel size) and 136 ms for partial brain acquisition (4×4×6 mm^3 voxel size) on a conventional clinical 3T scanner equipped with 12-channel head coil. Real-time image reconstruction was implemented using in-plane reconstruction with GRAPPA on the scanner and reconstruction in the 3rd spatial dimension on an external workstation enabling real-time fMRI analysis with time delays of less than 500 ms.

A central goal of this study was to compare BOLD sensitivity (mean and maximum percent signal change, mean and maximum t-score, extent of activation and temporal signal-to-noise ratio (tSNR)) of multi-slab EVI and conventional EPI across several tasks that engage functional brain networks in visual, auditory, motor and frontal cortex. A secondary goal was to quantify further improvement in BOLD sensitivity when applying a time domain filter that reduces physiological noise from cardiac and respiratory fluctuations (Lin et al 2011) while maintaining an effective temporal resolution comparable to that of EPI. We also wanted to assess the feasibility of mapping major resting state networks (RSN) at 136 ms temporal resolution, as previous work has shown that the sensitivity of mapping RSNs improves with increased sampling rates compared to conventional EPI (Feinberg et al 2010).

MATERIALS AND METHODS

Fifteen healthy subjects participated after giving institutionally reviewed informed consent. Data were collected on a clinical 3T scanner, MAGNETOM Trio, A Tim System (Siemens Healthcare, Erlangen, Germany) equipped with MAGNETOM Avanto gradient system and 12-channel array receive-only head coil. Pulse and respiration waveforms were recorded with 20 ms temporal resolution. Reconstructed 2D images were exported from the scanner reconstruction computer via the scanner host computer to an external Intel Xeon E5530, 6 core, 2.4 GHz workstation for reconstruction of the 3rd spatial dimension and real-time fMRI analysis, which were integrated into the in-house developed TurboFIRE software (Posse et al 2001).

Multi-slab EVI pulse sequence

The EVI pulse sequence, which was based on a multi-echo EPI (MEPI) sequence (Speck and Hennig 1998, Posse et al 1999) with flyback along the k_z-direction, is shown in Figure 1. Multiple adjacent slabs were excited sequentially and encoded in a single TR using repeated EPI modules with interleaved phase encoding gradients. The EPI modules consisted of trapezoidal oscillating gradients (G_{RO}) along the readout direction and a series of blipped primary phase encoding gradients (G_{PE1}) that were rewound at the end of every partition. A blipped secondary phase encoding gradient (G_{PE2}) that encodes the third spatial dimension was applied after each EPI module. K_z-space was encoded symmetrically using a dephasing gradient before the first EPI module ($k_{max}/2$). The k_x-k_y space trajectories for each k_z step were traversed in the same direction using 4-fold acceleration for GRAPPA reconstruction (Griswold et al 2002). Twenty-four GRAPPA auto-calibration signal (ACS) lines for in-plane GRAPPA reconstruction were acquired in a separate prescan using 4 interleaves.

Image distortion and BOLD contrast characteristics

Encoding of 8 slices per slab with 64×64 in-plane matrix was performed using 4-fold GRAPPA acceleration, 6/8 partial phase encoding, 2790 Hz/pixel readout bandwidth, trapezoidal readout gradients with ramp sampling and 4 mm in-plane resolution. The minimum effective TE of 28 ms for this readout corresponds to the TE routinely used with EPI sequences in our lab, which minimizes signal drop-out in the frontal lobe. The effective bandwidth per pixel in the slice direction and the in-plane phase encoding direction were 19 Hz/pixel and 149 Hz/pixel, respectively. The corresponding readout duration was 52 ms, which is approximately 1.3 x T_2* in cortex and provides close to optimum BOLD sensitivity as shown in our previous studies of multi-echo EPI (Posse et al 1999), while minimizing the degree of geometrical through-plane distortion in the frontal lobe. Geometrical distortion was computed using Eq. 4 in (Jezzard et al 1995):

$$d_{pixel}(x,y,z)=\gamma\Delta B_0(x,y,z)T_{acq}, \quad (1)$$

where γ is the gyromagnetic ratio and T_{acq} is the sampling time. For a maximum magnetic field inhomogeneity of 0.6 ppm in the ventral prefrontal cortex, the calculated displacement was 3.9 pixels along the slice direction and 0.5 pixels along the in-plane phase encoding direction.

Blurring of the point spread function in the slice direction due to signal relaxation was computed using Eq. 13.60 in (Haacke et al 1999):

$$FWHM_{T_2^*}=\frac{\sqrt{3}}{\pi}\frac{T_{acq}}{T_2^*}\Delta x \quad (2)$$

The calculated blurring in the slice encoding direction of multi-slab EVI for a typical T_2* value of 40 ms at 3T is 72 % of the voxel size. Blurring along the in-plane phase encoding direction in multi-slab EVI is less than 10 %. The corresponding blurring along the phase encoding direction in EPI is 36 % of the voxel size.

The elongated readout of multi-slab EVI increases the effective echo time and as a consequence the BOLD contrast for small structures compared to EPI. The effect of the long multi-slab EVI readout on BOLD contrast can be computed as a function of k_z using Eq.3 in (Posse et al 1999):

$$\Delta S(t) = S_0 \frac{t}{T_2^*} e^{-\left(\frac{t}{T_2^*}\right)\frac{\Delta T_2^*}{T_2^*}} \quad (3)$$

Using a typical T_2* value of 40 ms at 3T the BOLD contrast for the first k_z encoding step with effective TE of 5 ms is only 30 % of the maximum at TE 40 ms, whereas BOLD contrast for the last k_z encoding step with effective TE of 55 ms is 95 % of the BOLD effect maximum. This difference in BOLD contrast for high k_z values increases the effective echo time for small structures. The corresponding BOLD contrast difference for high k_y values in the standard EPI sequence is smaller (70 % and 100 %, respectively), which results in a smaller increase in the effective echo time and smaller BOLD contrast enhancement for small structures.

Using 4-fold k_y-space undersampling with 256 mm target FOV resulted in approximately 3-fold aliasing of the brain with typical head sizes. The “effective” GRAPPA acceleration in this configuration was thus 3-fold, which results in acceptable parallel imaging noise enhancement (Wiggins et al 2007). EVI reconstruction performance is further improved due to the high SNR afforded by the slab selection compared to EPI. Numerically optimized slab selection RF pulses and spatial oversampling of 1 slice on either side of each slab were used to minimize inter-slab crosstalk, to avoid spatial aliasing and to minimize signal losses at the slab edges. The bandwidth of the RF excitation pulse was increased almost 2-fold (time-bandwidth product: 10) and the duration of the RF pulse was decreased 4-fold from 2560 μs of the product sequence down to 640 μs to improve the slice profile and to minimize chemical shift and susceptibility-related slab displacement.

Data acquisition

High-resolution T_1-weighted MPRAGE (Magnetization Prepared RApid Gradient Echo) scans were acquired for spatial referencing using TR: 1810 ms, TI: 900 ms, TE: 2.52 ms, flip angle: 8°, bandwidth: 651 Hz/Px, 160 or 192 sagittal slices with 256×256 in-plane resolution, and isotropic 1 mm voxel dimensions. Multi-slab EVI data were acquired with two different temporal resolutions:

- **i.** TR: 286 ms, TE_{eff}: 28 ms, α: 10°, 4 slabs in AC/PC orientation, interleaved acquisition order, slab thickness: 24 mm, inter-slab gap: 10 %, matrix per slab: 64×64×8, Field of View (FOV) per slab: 256×256×32 mm^3, reconstructed isotropic voxel dimensions: 4 mm, scan time: 172 s, no. of scans: 600 for experiments 1 and 462 scans for experiment 2 (see below).
- **ii.** TR: 136 ms, TE_{eff}: 28 ms, α: 10°, 2 slabs in AC/PC orientation, slab thickness: 42 mm, inter-slab gap: 10 %, matrix per slab: 64×64×8, FOV per slab: 256×256×48 mm^3, reconstructed voxel dimensions: 4×4×6 mm^3. Task activation data were acquired with scan times of 160 s using 1176 scan repetitions. Resting state data were acquired with scan time of 4 min and 59 s using 2199 scan repetitions.

Fully sampled EPI data were acquired using identical TE, voxel size and scan time as 4-slab EVI data, and TR: 2 s. The total number of scans was 84 for experiment 1, and 66 for experiment 2. Thirty two slices with 0% gap were acquired using interleaved acquisition order.

Multi-slab EVI and EPI data sets were acquired in a phantom with internal grid structures, the dimensions of which were on the order of the voxel size, to compare spatial resolution and geometrical distortion. Signal instability during 5 min scans was measured using a

homogeneous cylindrical phantom. Measurements were started after allowing adequate time for stabilization.

Activation studies

Paradigm presentation was programmed using ePrime software (Psychology Software Tools, Inc., Pittsburgh, PA). Visual stimulation was provided using an in-house built MR compatible projection system. Auditory stimulation was delivered using an MR compatible headset (Avotek Inc., Stuart, FL). An in-house developed button-response device (MIND Research Network, Albuquerque, NM) was employed to monitor motor task execution. Subjects were instructed to attend to each task with a constant effort across scans.

Experiment 1—Four subjects performed simultaneous visual and motor tasks using a block design paradigm. The visual activation task was eyes open in the lit scanner environment versus eyes closed. The motor task consisted of 2 Hz right hand index finger tapping versus rest. Subjects were asked to tap with maximum extension of the index finger. Start and stop of task execution was initiated by short beeps. The task duration was 4 s and the interstimulus interval was 23. The tasks were repeated 5 times. Data were acquired with 4-slab EVI using a TR of 286 ms and with EPI using a TR of 2 s.

Experiment 2—Three subjects performed a multi-task paradigm that consisted of four interleaved tasks: visual (checkerboard stimulation), motor (2 Hz right index finger tapping), auditory (syllable discrimination), and cognitive (mental calculation). These tasks were arranged in a randomized block design (8 s per block), with a crosshair serving as baseline for a total of 132 s per scan. The total duration for each condition was thus approximately 27 s. Visual stimulation consisted of black and white checkerboards. Finger tapping in the motor task was paced with an auditory tone (1 kHz). Subjects were asked to tap with maximum extension of the finger. During the auditory task, subjects listened to recorded syllables (i.e., “Ah, Ba, Ha, Ka, Ra, …”) and pressed a button when they heard the target syllable “Ta” (25% of syllables). The cognitive task consisted of mental calculations. Subjects were asked to sum three aurally presented numbers and divide the sum by three, responding with a button press when the sum was integer-divisible by three (50% of trials). Data were acquired with 4-slab EVI using a TR of 286 ms and with EPI using a TR of 2 s.

Experiment 3—Three subjects performed simultaneous visual and motor tasks using a block design paradigm. Visual stimulation consisted of checkerboard display versus crosshair. The motor task consisted of 2 Hz right hand index finger tapping versus rest. Subjects were asked to tap with maximum extension of the index finger. Start and stop of task execution was initiated by short beeps. The task duration was 4 s and the interstimulus interval was 23. The tasks were repeated 5 times. Data were acquired with 2-slab EVI using a TR of 136 ms.

Experiment 4—Four subjects participated in resting state scans (eyes open), which lasted 4 min and 59 s. They were instructed to relax, clear their minds and fixate on a crosshair. Data were acquired with 2-slab EVI using a TR of 136 ms. Resting state data in two additional subjects were measured using EPI and multi-echo EPI with TR: 2 s. The fourth echo, which corresponds to conventional EPI, was extracted.

Multi-slab EVI image reconstruction

The reconstruction pipeline used distributed computing across the scanner using the ICE environment and the external workstation using the custom fMRI research tool TurboFIRE (version v.5.10.0.1) (Posse et al 2001). In-plane (k_x, k_y) reconstruction of complex (magnitude and phase) images for each encoded k_z step and slab was performed online on

the scanner. Real-time export of magnitude and phase images to the external workstation was performed using the ACE library for TCP/IP communication and socket stream (http://www1.cse.wustl.edu/~schmidt/ACE.html). Image transfer to the scanner image database was disabled for performance reasons. Image reconstruction in the k_z dimension on the external workstation included Hamming filtering, Fourier transformation, slice ordering and concatenation of stacks of slices from different slabs to form contiguous 3D image volumes. The time delay from acquisition to display of reconstructed images was less than TR.

Slice ordering consisted of the following steps: (i) The offset D of the stack of slabs from the magnet center was computed based on the slab prescription on the scanner console, which includes the offset of the center of the slabstack P with respect to the magnet center along the principal axes: right-left (RL), anterior-posterior (AP) and head-foot (HF), and the slab rotation angles α around the RL axis and β around the AP axis, as well as the slice thickness (SLT). This involves computing the normal unit vector of the slabstack ($\vec{n}$) using Euler rotation matrices, projecting the position vector $\vec{p}$ onto $\vec{n}$ (Figure 2), and adjusting a half-slice offset to account for the digitization of the slices:

$$D = RL\cos(\alpha)\sin(\beta) - AP\sin(\alpha) + HF\cos(\alpha)\cos(\beta) - 0.5 \cdot SLT \quad (4)$$

(ii) D determines the aliasing of reconstructed slices along the slice direction within the encoded FOV (FOV_z), which was accounted for by a circular shift of the stack of slices for each slab. (iii) Slices at the edge of the slab were included, if their overlap with the slab exceeded a user-selected fraction of the slice thickness (30 %).

Data analysis

Spatial resolution in multi-slab EVI and EPI images was assessed by comparing the full width at half maximum of the grid structures in the phantom images. An approximation of the spatial signal-to-noise ratio was obtained by computing the ratio of the mean signal intensity inside the phantom or brain and the standard deviation of noise outside of the phantom or brain in a region that was free of ghosting, scaled by 0.655 to account for the Rayleigh distribution of signals within the noise region.

Signal instability in phantoms was measured as described in Weisskoff 1996. The standard deviation of signal fluctuations over time was measured as a function of the length of a square region of interest (ROI) in a central slice of the phantom data and compared with the single image SNR. 2nd order detrending was applied. Region dimensions ranged from 1×1 to 32×32 voxels. The relative fluctuations and the theoretical SNR limits were plotted as a function of ROI size.

Online and offline fMRI analysis was performed using the custom fMRI research tool TurboFIRE (Posse et al 2001). Preprocessing included performance-optimized rigid body motion correction (Mathiak et al 2001) with online display of motion parameters, slice time correction in case of EPI and spatial normalization into MNI space (Gao et al 2003). EVI data were additionally processed with a moving average digital filter. The filter width was chosen to be 2 s, which was shown to be optimal for estimating the hemodynamic response (Lin et al 2011) and coincides with the TR of the EPI data. Image data were segmented into 144 functional brain regions in Talairach space based on the Talairach Daemon database and Matthew Brett's formula (Gao et al 2003). Statistical analysis consisted of simultaneous cumulative general-linear-model (GLM) analysis (Bagariano et al 2003) with up to 6 individually modeled reference vectors convolved with a canonical 6 parameter hemodynamic response model. Correction for temporal correlations was not available.

Cummulative correlation analysis (Gembris et al 2000) was performed for comparison. Activation maps were spatially smoothed using a 3×3 median filter. During real-time scanning up to 6 signal time courses from either manually selected ROIs or automatically selected VOIs were displayed using the 144 predefined functional areas.

The normalized raw image data and the t-maps for experiments 1 and 3 were labeled with Talairach coordinates for each voxel, automatically segmented into 144 predefined functional areas and further processed using scripts written in Perl (http://www.perl.org/). The maximum and the mean BOLD signal amplitude (average of percent signal change from baseline to maximum BOLD signal in individual blocks of activation), the maximum and the mean t-score, and the extent of activation were measured in visual cortex (BA17-19) and in extended motor cortex (BA1-6). Voxels with less than 50 % of maximum signal intensity within target regions were excluded to remove edges. For experiment 1 only voxels that were consistently activated in all EVI and EPI scans of a given subject were selected for measuring percent signal change and t-scores to ensured identical VOI selection across all EVI and EPI scans of a subject. The t-score threshold for activation detection in visual cortex was 5.0, which was identical to the threshold employed in SPM8 for a p-threshold of 0.001 that was corrected for multiple comparisons (see below). In the extended motor cortex the selected t-threshold was 3.0 to ensure adequate voxel statistics.

The temporal signal-to-noise ratio (tSNR), which is defined as (Murphy et al 2007):

$$\mathrm{tSNR}=\mu/\sigma \tag{5}$$

where μ is the mean signal and σ is the standard deviation across the time domain, was computed on a voxel-by-voxel basis in left Brodmann Area 10 (BA 10 L) for non-activated voxels with t-scores less than 1.0. Left BA10 was selected, since it did not show paradigm related signal changes as verified by correlation and ROI analysis.

A subset of 4-slab EVI and EPI scans obtained with experiment 1 were processed with SPM8 (http://www.fil.ion.ucl.ac.uk/spm/) for comparison with TurboFIRE analysis. Processing steps included concatenation of all EVI and of all EPI scans measured in a single subject, motion correction, correction for slice timing in case of EPI, spatial normalization, spatial smoothing with 8 mm Gaussian kernel, inclusion of the first derivative of the main effect in the design matrix and first order autoregressive modeling. Maximum t-scores and extents of activation of the largest cluster were computed using a p-threshold of 0.001 that was corrected for multiple comparisons.

For experiment 2 the maximum t-scores and extents of activation in visual cortex (BA 17–19), in motor cortex (BA 1–3), in auditory cortex (BA 21 and 22) and in frontal cortex (including BA 4, 6–11, 32, 40 and 46) were computed using cluster analysis in TurboFIRE with a t-threshold of 5.0.

Spatial independent component analysis (ICA) of the data collected in experiment 4 was performed using the GIFT software package v1.3i (http://mialab.mrn.org/software/gift/). Preprocessing using SPM8 (http://www.fil.ion.ucl.ac.uk/spm/) consisted of motion correction, coregistration with the EPI.mni template and spatial normalization to ensure consistent multi-session and/or multi-subject analysis. No spatial smoothing was applied. The ICA algorithm used throughout was FastICA introduced by Hyvarinen and Oja (Hyvarinen and Oja 1997), since it had previously been shown to be more robust and computationally efficient compared with the competing alternative approaches for fMRI data analysis (Mutihac and Van Hulle 2004). The settings used for all data sets were the following: epsilon: 10^{-6}, maximum number of iterations: 1024, maximum number of fine-tuning sessions: 64, using tanh as the nonlinear transfer function, sample size: 1, deflation

mode, stabilization: on, and pow3 as “g” function. In order to estimate the data subspace (model selection), minimum description length (MDL) was applied to the raw data. The validation of ICA decomposition was carried out by running ICASSO (http://www.cis.hut.fi/projects/ica/icasso/) for each subject, so that the most stable directions were selected after statistical resampling (bootstrap) of the raw data. Principal Component Analysis was used for prewhitening based on singular value decomposition. A Z-threshold of 1.5 was used to map independent components. The maximum Z-scores in each component was measured. Independent components representing the 5 major resting state networks (RSNs) were identified by visual inspection in reference to the Talairach brain atlas using spatial and temporal selection criteria described in previous studies (De Luca et al 2006, Schoepf et al 2010). RSNs were identified by slowly modulated signal time courses that were well above noise level with Z scores greater than 5.0. The five major RSNs then were classified spatially by the following regional anatomy (De Luca et al 2006):

1. RSN1 (occipital): a posterior network characterized by involvement predominantly of occipital cortex, as well as temporal–parietal regions;
2. RSN2 (default mode): a posterior lateral and midline network involving primarily the precuneus and anterior pole of the prefrontal lobe, as well as parietal regions.
3. RSN3 (bilateral sensorimotor): a lateral and midline network including the pre- and post-central gyri, as well as midline regions including the thalamus and hippocampus.
4. RSN4 (dorsal parietal and lateral prefrontal): a network involving dorsal parietal and predominantly lateral prefrontal cortex.
5. RSN5 (temporal): a ventral network dominated by coherences between the inferior occipital parietal, temporal, and inferior prefrontal cortices.

Statistical analysis

Mixed linear models with a fixed effect of scan type and random intercepts with unstructured covariance structure were fit to account for the unbalanced repeated measures among subjects. If the null model likelihood ratio test had an insignificant chi-square, then the random intercept was dropped from the model and only the fixed effect was retained. P-values for comparisons between scan types were estimated from the least squares means estimates and the Scheffé correction for multiple comparisons was used where warranted. A limitation of this method is the assumption of normality in these small sample sizes; however, limited methodology exists for small-sample unbalanced repeated measures ANOVA and this analysis proved to be the most robust among alternatives. When plotted, the data appeared to be approximately normally distributed. Significance was held at $\alpha = 0.05$. All analysis was performed in SAS v. 9.3.

Results

Image quality and reconstruction performance

The in-plane geometrical distortion of 4-slab EVI measured in a phantom with internal grid structures was small, comparable to that of EPI (Figure 3). Through-plane geometrical distortion was visible in the outermost slices of 4-slab EVI (Figure 3e). The displacement in the center of these slices was approximately one slice thickness (4 mm) relative to the outer edge. Spatial blurring in-plane was similar to that of EPI. Through-plane spatial blurring was approximately 1 slice thickness (4 mm), which is roughly consistent with theoretical estimates. In-plane ghosting was less than 5%, similar to that of non-accelerated EPI.

Signal instability measured in the cylindrical phantom indicates that the effect of scanner instability on tSNR in 4-slab EVI was comparable to EPI, while the relative contribution of scanner instability to signal fluctuations was slightly smaller for 2-slab EVI (Figure 4). Oscillatory signal intensity fluctuations up to 2% peak-to-peak with a periodicity of 0.5 Hz were measured at the edges of the slabs, reflecting steady-state effects. Signal drift and displacement along the slice direction due to gradient heating was minor.

Figure 5a shows the typical placement of the 4-slab EVI in the human brain. Geometrical distortions were mostly restricted to the ventromedial prefrontal cortex, which was imaged by the most inferior slab (Figure 5b). Through-plane displacement in that slab was typically on the order of 1 slice or less, but in some subjects the displacement was up to 2 slices, which lead to localized wrap-around effects in the slice direction. EPI exhibited slightly larger in-plane distortion in the prefrontal cortex than 4-slab EVI (Figures 5d and 5e). Four-slab EVI and conventional EPI displayed similar in-plane resolution and image uniformity in most slices in upper cerebrum (Figure 5, f and g). Signal dropout in ventromedial prefrontal cortex was comparable to EPI. Flip angle dependence of BOLD contrast was characterized in vivo at a TR of 286 ms. FMRI sensitivity was slightly larger at 30° flip angle compared to 10° and 90° flip angle, which is close to the Ernst angle (37°) in gray matter at 3 Tesla. However, a 10° flip angle was chosen for both TR: 286 and TR: 136 ms (Ernst angle in gray matter: 26°) to minimize both in-flow effect and signal saturation in CSF spaces at the expense of SNR. As a consequence, high image contrast between brain tissue and ventricles was obtained. Volume coverage with 4-slab EVI (25 reconstructed slices) encompassed upper cerebrum and cerebellum. The gap between the slabs caused three of the reconstructed slices to be 20–40% darker than the adjacent slices depending on the position of the gaps between slabs relative to the encoded slice. After spatial normalization into MNI space multi-slab EVI data were almost indistinguishable from normalized EPI data.

A range of image resolutions, matrix sizes and slab orientations was investigated: Although a minimum in-plane resolution of 3 mm was technically feasible, a significant increase in g-factor related noise in the center of the FOV due to the limited spatial encoding capabilities of the 12-channel coil was noted. A 4 mm in-plane resolution was chosen as a compromise to ensure acceptable g-factor related noise enhancement and to minimize ghosting. Acquisition of a larger image matrix with up to 12 encoded k_z-space lines was investigated: Acceptable image quality was obtained with 64×64×12 matrix and an effective TE of 43 ms: however, increased blurring, ghosting and signal dropout in ventral prefrontal cortex were noted. Data acquired in sagittal orientation were comparable in quality to axially acquired data. However, axial data acquisition was preferred to compare with standard EPI protocols used in our laboratory and for partial brain acquisition in the upper cerebrum with TR: 136 ms. Performance tests showed that data acquisition, in-plane image reconstruction of magnitude and phase images, image transfer to the external workstation, reconstruction in the slice direction and real-time fMRI analysis with ROI analysis could be sustained with data rates of up to 235 2-dimensional images/s (magnitude and phase). The steady-state time delay between data acquisition and update of the activation maps at TR: 136 ms was less than 0.5 s.

BOLD sensitivity comparison between 4-slab EVI and EPI

Experiment 1—Figure 6 shows an example of SPM8 analysis comparing three concatenated 4-slab EVI scans without moving average filter and three concatenated EPI scans in a single subject. With 4-slab EVI a maximum t-score of 108.7 in the visual cortex and larger spatial extent of activation (138.4 cc) was measured compared to a maximum t-score of 23.6 and extent of 106.1 cc in EPI. This difference in t-scores was also measured in

single scans. Application of the moving average filter further increased the t-scores of 4-slab EVI data. Figure 5 shows a comparison between single scan 4-slab EVI data with moving average filter and single scan EPI data.

The results in individual scans, which are listed in Tables 1–4, were as follows: The mean and maximum BOLD signal amplitude and mean and maximum t-scores in the visual cortex (Brodmann areas 17–19) were significantly larger with 4-slab EVI compared with conventional EPI (Table 1). The maximum signal changes in some voxels exceeded 10%, which may reflect BOLD effect in large blood vessels. Similar results were obtained in the extended motor area (Brodmann areas 1–6). The increases in BOLD signal amplitude with 4-slab EVI relative to EPI were larger than those in the visual cortex. However, the increases in t-scores with 4-slab EVI relative to EPI were smaller than those in the visual cortex.

The moving average filter significantly increased the mean and maximum t-scores in the visual and the motor cortex (Table 2). The spatial extent of activation in both areas was significantly larger for 4-slab EVI with moving average filter comparted to EPI (Table 3). The moving average filter broadened the signal response and reduced the mean and maximum BOLD signal amplitude. In visual cortex the BOLD signal amplitude became similar to that measured with EPI (Table 1). In motor cortex the mean and maximum BOLD signal amplitude remained significantly higher than with EPI (Table 1).

The average temporal signal-to-noise ratio in left Brodmann area 10, in voxels which were not activated by this task, was 52.1% smaller using 4-slab EVI compared to EPI (Table 4). After moving average filtering this difference reduced to 24.3 %. The tSNR across the entire brain, which was measured in one subject, was 128.3. The tSNR in left Brodmann area 10 in this subject was 90.0. The difference in spatial SNR was not significant: 4-slab EVI had an average spatial signal-to-noise ratio (SNR) of 209 +/− 26, whereas EPI had an average spatial SNR of 207 +/− 18.

Experiment 2—This experiment using rapid switching between multiple tasks to engage a larger range of functional networks confirmed the observation in experiment 1 (Table 5). Maximum t-scores were 2–3 times larger with 4-slab EVI compared to EPI. Extents of activation were 3–15 times larger with 4-slab EVI compared to EPI, depending on brain region. In visual and auditory cortex these differences were statistically significant. Increases in extent of activation in motor and frontal cortex did not reach statistical significance due to inter-scan and inter-subject variability. This is in part due to the increased complexity of this interleaved task design compared to experiment 1, which is sensitive to variation in reaction time and changes in attention associated with task switching.

BOLD sensitivity using 2-slab EVI at TR 136 ms

Experiment 3—Strong signal changes well above noise level of the same magnitude as with 4-slab EVI were measured in single trials (Figure 7). The results in individual scans, which are listed in Tables 6–8 were as follows: Mean BOLD signal amplitude in Brodmann areas 17–19 and mean and maximum BOLD signal amplitude in Brodmann areas 1–6 were in a similar range as those measured with 4-slab EVI (Table 6). Mean and maximum t-scores, and extents of activation in these areas were smaller than those measured with 4-slab EVI (Table 7). The average temporal signal-to-noise ratio in left Brodmann area 10, in voxels which were not activated by this task, was 19% smaller than with 4-slab EVI (Table 8). The moving average filter significantly increased the mean and maximum t-scores, the extent of activation and the temporal signal to noise ratio, but significantly reduced the mean and the maximum BOLD signal amplitude, consistent with the results obtained using 4-slab EVI. The average spatial SNR was 239 +/− 23.

The fast sampling rate improved detection of cardiac related physiological noise components in the brain stem, in the insular cortex and in CSF containing spaces (Figure 8) and signal fluctuations correlated with respiration. The physiological recordings enabled unambiguous identification of physiological noise components in ICA analysis. Comparison of the pulse recordings and the signal time couses in cardiac-related ICA components showed that the time delays between corresponding pulsations in the two data traces were highly consistent during the entire duration of a scan. The power spectra of pulse recordings and cardiac-related ICA components (Figure 8e) were similar up to the 2nd harmonic.

Non-task related signal changes in the visual cortex well above baseline (Figure 7c), which may reflect visual imagery, were also detectable. In single trials the 6-parameter canonical hemodynamic response function implemented in TurboFIRE, which is based on SPM99, provided a good fit of the BOLD signal time course, but deviations from the canonical response function due to variability in reaction time were noted (Figure 7c). Non-task-related brain activation, such as visual imagery and visual after-effects, were also detectable in the time course. One of the subjects reported a strong negative afterimage of the checkerboard, which persisted for several seconds and was clearly detectable as a prolonged hemodynamic response in single trials. Furthermore, the fast acquisition speed of multi-slab EVI reduced the effects of intra-scan movement and improved the identification of non-BOLD noise sources. For example, small sub-second head movement was clearly identifiable in the displacements and rotations that were plotted by the motion correction in TurboFIRE.

Detection of resting state networks using 2-slab EVI

Experiment 4—The ICA decomposed individual subject scan 2-slab EVI data into 25 to 32 components. The five major resting state networks RSN1-5 described by De Luca et al in 2006 were consistently detected in all subjects in single scans (Figure 9). These RSNs were associated with clearly identifiable slowly varying signal time courses well above noise level with mean Z-scores of 11.8 +/− 2.7 (Table 9). Four additional minor RSNs with activation encompassing parietal, occipital, lateral prefrontal, temporal and inferior frontal regions (RSN6-9) were also detected, but less consistently across subjects. The majority of remaining components depicted physiological signal fluctuation due to cardiac pulsation and respiration in insular cortex, brain stem and CSF, and head movement related signal changes in the periphery and at the edges of the slabs. The remainder of the components represented artifacts, such as occasional spikes and slow signal drifts. The 5 major resting state networks were also detected in conventional EPI, but some of the spatial maps were noisier than with 2-slab EVI and the signal modulation in the ICA time courses was less distinct from background noise compared with 2-slab EVI (Figure 9).

The detection of RSNs in 2-slab EVI data as a function of the total number of selected ICA maps was also investigated. Reducing the number of selected components to 14 in 2 of the subjects removed RSNs 6–9, which were merged into other components. It also removed RSN4 in one of the two subjects. A secondary goal was to investigate whether the 5 major resting state networks in 2-slab EVI data were detectable in shorter scan times. Time series data from all subjects were separated into two segments with 1100 scans corresponding to 2 min 30 s scan time and into 4 consecutive segments with 550 scans corresponding to 75 s scan time. On average, RSN1 was detected in 63 % of the 2 min 30 s segments and 56 % of the 75 s segments, RSN2 was detected in 88 % of the 2 min 30 s segments and 50 % of the 75 s segments, and RSN3 was detected in 50 % of the 2 min 30 s segments and 31 % of the 75 s segments (Figure 10).

Discussion

Sensitivity

Multi-slab EVI significantly increases t-scores of activation and BOLD signal amplitude compared to EPI, not only in large blood vessels, but also across extended functional areas in visual, motor and auditory cortex. These gains are expected to extend to frontal cortex, although they did not reach statistical significance in this study due to intra-subject variability in task performance. The high temporal resolution of multi-slab EVI enabled the use of a time domain moving average filter, which was recently described by Lin et al 2011, to reduce physiological signal fluctuations and to further increase t-scores and extent of activation compared to EPI, while maintaining an effective temporal resolution comparable to that of EPI. The relative gains in t-scores measured with the filter were in a similar range as those reported by Lin et al 2011.

The increase in BOLD signal amplitude was in part due to the longer readout duration of 1.3 * T_2*, which provides close to maximum BOLD sensitivity as shown for multi-echo EPI (Posse et al 1999), while limiting geometrical distortion and blurring of the point spread function in the slice direction compared to conventional single-shot EVI. The long readout also increases the effective echo time for small structures, which increases BOLD contrast in focal areas of activation. The increases in BOLD signal amplitude compared to EPI were strongest in motor cortex, which exhibits more focal activation compared to visual cortex. These differences remained significant in the motor cortex even after moving average filtering, but not in the visual cortex.

This increase in t-scores is in part due to the improved Nyquist sampling of cardiac and respiration related signal fluctuation, which are major noise sources at high field strength (Krüger and Glover 2001, Triantafyllou et al 2005). The fast sampling rate also more than compensates for the moderate 52% reduction in temporal SNR of 4-slab EVI compared to EPI.

The lack of autoregressive modeling in our data analysis introduces possible bias due to temporal correlations in the noise. The high temporal resolution of multi-slab EVI increases the number of time points by almost an order of magnitude compared to conventional EPI, which with standard GLM analysis and without prewhitening increases the t-scores. SPM8, which was applied in our data analysis for comparison with the TurboFIRE pipeline, uses an AR(1) model for correcting temporal correlations, which may not be adequate for controlling the strong auto-correlations in multi-slab EVI data. Several papers, including an often-cited publication by Worsely et al 2002, have addressed higher order temporal correlations in fMRI. A recent publication by Lin et al 2010 adapted Worsely's approach of prewhitening to remove temporal correlations in the noise for InI-based high-speed fMRI. In a preliminary analysis we investigated the effect of prewhitening using the FSL software package (http://www.fmrib.ox.ac.uk/fsl/). In case of 2-slab EVI data prewhitening reduced the t-scores by as much as 42 % compared to data processed without prewhitening. We are currently studying temporal correlations in multi-slab EVI data in the context of univariate autoregressive models to determine the appropriate model order (Mutihac et al 2011). Preliminary results suggest that a 6^{th} order model might be appropriate for 4-slab EVI data. However, while autoregressive modeling and assessment of tools for temporal prewhitening are part of ongoing method development, these investigations are beyond the scope of the present study.

In the absence of appropriate noise models in our data analysis methodology we estimated an upper bound for the effect of the increased sampling rate on the t-scores using the 4-slab EVI data analyzed with the moving average filter. Assuming that the moving average filter

introduces strong temporal correlations, which reduce the effective degrees of freedom of 4-slab EVI to those of EPI (an overestimation), the t-scores measured with the moving average filter in Table 2 were rescaled using a correction factor of $\sqrt{TR_{EVI}/TR_{EPI}}$. The rescaled mean and maximum t-scores in visual cortex were still 12% and 82% larger than those of EPI. The rescaled mean t-score in motor cortex was similar to that of EPI, while the rescaled maximum t-score was still 13% larger than those of EPI. These results suggest that the increase in t-scores with multi-slab EVI can only in part be explained by an apparent increase in degrees of freedom due to the high sampling rate alone.

Multi-slab EVI is also considerably less sensitive to physiological noise than segmented 3D EPI methods (Poser et al 2010), which are affected by signal fluctuations between segments that lead to signal incoherence in k-space. These lead to ghosting and increase apparent physiological signal fluctuation. Multi-slab EVI employs significantly longer TR than segmented 3D EPI methods, which further increases the sensitivity advantage and reduces steady state effects.

Signal decreases at the intersections of slabs introduce heterogeneity in spatial coverage and BOLD sensitivity. To address this issue it is necessary to further optimize slab selection using excitation methods with much sharper transition bands, such as variable rate selective excitation (VERSE) (Hargreaves et al 2004). Nonetheless, some degree of transition band overlap will be unavoidable. We are currently investigating to which extent averaging of slices in the transition region that are encoded in adjacent slabs would minimize overall signal losses.

Temporal resolution

Compared to single-shot EVI the temporal resolution is reduced, which is primarily due to the repetitions of the lipid suppression and excitation modules for each slab and due to spatial oversampling in the slice direction within each slab. Spatial oversampling of the slab is associated with a 25% increase in acquisition time in our current method implementation using 8-slice encoding across a slab that covers 6 slices. Larger matrix size in the k_z-direction up to 16 slices is feasible with our method at the expense of increased effective TE. To further increase temporal and spatial resolution and volume coverage, we are investigating 2-dimensional parallel imaging in conjunction with a 32 channel array coil. This would enable whole brain multi-slab EVI with a TR, which approaches that of single-shot EVI. Further increases in temporal resolution approaching that of InI to improve deconvolution of physiological noise will be feasible using superresolution reconstruction (Otazo et al 2009). It may be possible to measure multiple consecutive EVI trajectories in a single shot thus enabling quantification of T_2* and further increasing BOLD sensitivity using weighted combination of these EVI data sets. It will be of interest to compare the BOLD sensitivity of multi-slab EVI with that of other high-speed fMRI methods, such as multiplexed EPI, which provides excellent image quality at moderate temporal resolution on the order of 100s of ms, and Inverse Imaging (InI) and variants thereof with partial gradient encoding, which have achieved much higher temporal resolution (Lin et al 2006, Lin et al 2008, Lin et al 2010, Zahneisen 2011).

The fast sampling of the physiological noise is advantageous for precisely characterizing the onset, peak time and decay of task-related BOLD signal changes in individual nonaveraged trials and for identifying non-task related BOLD signal changes. As our data show it is possible to measure the time course of task-related signal changes well above noise level in single non-averaged trials that closely match the commonly employed canonical hemodynamic response model employed in SPM8 (Josephs et al 1997), leading to very high correlation coefficients and t-scores. This high contrast-to-noise ratio and the high temporal

resolution of multi-slab EVI are thus suitable for characterizing differences in hemodynamic onset times between brain regions, which has been the topic of several recent studies to assess functional connectivity (Lin et al 2008, Lin et al 2010). The high temporal resolution of multi-slab EVI eliminates the need to jitter the onset of individual events in event-related studies and enables precise measurements of cardiac- and respiration-related signal fluctuation in different brain regions. Adding the time courses of physiological noise components based on peripheral recordings or ICA time courses to the GLM design matrix will enable sensitive mapping of physiological signal fluctuations. We currently investigating to which extent this approach increases sensitivity for mapping task-related activation.

Spatial resolution, geometrical distortion and movement sensitivity

The high temporal resolution and sensitivity of multi-slab EVI comes at the price of increased geometrical distortion in the slice direction in the ventromedial prefrontal cortex and spatial blurring of the BOLD response compared to EPI. Multi-slab EVI represents a compromise that provides high sensitivity while limiting geometrical distortion and spatial blurring at only moderate reduction of acquisition speed compared to single-shot EVI. The spatial resolution in our current implementation is limited by the spatial encoding capabilities of the 12-channel head array coil. Using a 32-channel head array coil in conjunction with 2-dimensional parallel imaging would enable larger overall acceleration factors to achieve isotropic spatial resolution of 3 mm, which is more typical for fMRI studies, and reduction of g-factor related noise enhancement. Multi-slab EVI is particularly advantageous at high field strength, since it mitigates the gradient performance limitations that result in excessive readout durations with single-shot EVI.

Current work is aimed at correcting through-slice geometrical distortion, in particular in ventromedial prefrontal and temporal brain regions that suffer from strong magnetic field inhomogeneity. Comparing methods for correcting geometrical distortion in EVI, a previous study has found that deconvolution of the point spread function was most effective (Quian et al 2009). We are thus planning to integrate point-spread-function mapping (Zaitsev et al 2004) along the k_z-direction to reduce geometrical distortion. We are also investigating slab-specific shimming to further reduce geometrical distortion and signal losses, which is not feasible with whole brain single-shot EVI.

Although the high temporal resolution of multi-slab EVI minimizes intra-scan motion artifacts, the long readout makes multi-slab EVI more sensitive than EPI to movement related changes in magnetic field homogeneity, which manifest as geometrical distortion and image intensity changes. To minimize head movement related image distortion we are planning to implement prospective acquisition correction (PACE) (Thesen et al 2000) with dynamic shimming.

Resting state studies

Detection of five major RSNs in single subjects is facilitated by the high BOLD sensitivity and high temporal resolution of multi-slab EVI, which is consistent with a previous study by Feinberg et al 2010 using multiplexed EPI. Z-scores were higher than those measured with EPI in comparable scan times. Using the minimum description length criterion resulted in a relatively small number of ICA components relative to the large number of time points in an EVI scan. For EPI the number of ICA components is typically much larger relative to the total number of time points. This difference may be a reflection of the improved sampling of physiological noise sources with EVI, which improves separation of signal sources. At shorter simulated scans times we found that multiple RSNs were merged in single independent components, thus reducing measurement specificity. Our resting state data also

suggest that using a larger number of components than provided by the minimum description length criterion may be advantageous for separating RSNs, such as RSN3 and RSN5, that are co-localized in a single ICA map in our data, and requires further investigation. The high Z-scores of the major RSNs in our data and feasibility of detecting RSNs at much shorter scan times open up the possibility of directly measuring fluctuations in RSN activity, which will be the subject of a future investigation.

Conclusions

This study shows feasibility of high temporal resolution real-time fMRI using multi-slab EVI on a standard clinical MR scanner. The increased BOLD sensitivity of multi-slab EVI compared to multi-slice EPI is advantageous for real-time detection of event-related fMRI signal changes, for separation of physiological noise components and for detecting resting state networks in short scan times. High sensitivity for measuring brain activation in short scans is highly desirable for fMRI studies in children and in many clinical populations, such as patients with movement and neurodegenerative disorders. Multi-slab EVI has the potential to become an alternative to EPI as the accelerating development of parallel imaging and large-scale array coils transforms clinical imaging.

Acknowledgments

We gratefully acknowledge grant support from NIH (1 R01 EB002618-01, 1R41NS062474-01) and DoE/The MIND Research Network (DE-FG02-99ER62764), which supported part of this research. R.M. was supported by NAS/NRC Award #W81XWH-07-2-0001-0114 and Fulbright S&T Grant #495/2010. The statistical analysis was supported by the University of New Mexico Clinical and Translational Science Center, #1UL1RR031977-01. We thank Diana South for providing expert assistance with data collection, Abhishek Reddy Yeruva for assisting with data analysis, and Akio Ernesto Yoshimoto and Kwaku Akrofi for supporting the intial method development. We also thank Larry Wald, Thomas Witzel, Terran Lane, Fa-Hsuan Lin, Vincent Calhoun, Edward Bedrick and David Feinberg for inspiring discussions and critical feedback.

References

Bagarinao E, Matsuo K, Nakai T, Sato S. Estimation of general linear model coefficients for real-time application. Neuroimage. 2003 Jun; 19(2 Pt 1):422–9. [PubMed: 12814591]

Calhoun VD, et al. A method for making group inferences from functional MRI data using independent component analysis. Hum Brain Mapp. 2001 Nov; 14(3):140–51. [PubMed: 11559959]

De Luca M, Beckmann CF, De Stefano N, Matthews PM, Smith SM. fMRI resting state networks define distinct modes of long-distance interactions in the human brain. Neuroimage. 2006 Feb 15; 29(4):1359–67. Epub 2005 Nov 2. [PubMed: 16260155]

Edelstein WA, Glover GH, Hardy CJ, Redington RW. The intrinsic signal-to-noise ratio in NMR imaging. Magn Reson Med. 1986; 3(4):604–618. [PubMed: 3747821]

Feinberg DA, Moeller S, Smith SM, Auerbach E, Ramanna S, et al. Multiplexed Echo Planar Imaging for Sub-Second Whole Brain FMRI and Fast Diffusion Imaging. PLoS ONE. 2010; 5(12):e15710.10.1371/journal.pone.0015710 [PubMed: 21187930]

Friston KJ, Holmes AP, Poline J-B, Grasby PJ, Williams SCR, Frackowiak RSJ, Turner R. Analysis of fMRI time series revisited. NeuroImage. 1995; 2:45–53. [PubMed: 9343589]

Gao, K.; Posse, S. TurboFire: Real-Time fMRI with Automated Spatial Normalization and Talairach Daemon Database. Neuroimage; Proc. 9th Annual Meeting of the Organization of Human Brain Mapping; 2003. p. 838

Gembris D, Taylor JG, Schor S, Frings W, Suter D, Posse S. Functional MR Imaging in Real-Time using a sliding-window correlation technique. Magnetic Resonance Medicine. 2000; 43:259–268.

Griswold MA, Jakob PM, Heidemann RM, Nittka M, Jellus V, Wang J, Kiefer B, Haase A. Generalized autocalibrating partially parallel acquisitions (GRAPPA). Magn Reson Med. 2002; 47:1202–1210. [PubMed: 12111967]

Grotz T, et al. Fast functional brain imaging using constrained reconstruction based on regularization using arbitrary projections. Magn Reson Med. 2009 Aug; 62(2):394–405. [PubMed: 19526512]

Haacke, EM.; Brown, RW.; Thompson, MR.; Venkatesan, R. Magnetic Resonance Imaging: Physical Principles and Sequence Design. Wiley; Jun. 1999

Hargreaves BA, Cunningham CH, Nishimura DG, Conolly SM. Variable-rate selective excitation for rapid MRI sequences. Magn Reson Med. 2004 Sep; 52(3):590–7. [PubMed: 15334579]

Hyvarinen A, Oja E. Fast fixed-point algorithm for independent component analysis. Neural Comput. 1997; 9(7):1483–1492.

Hu Y, Glover GH. Three-dimensional spiral technique for high-resolution functional MRI. Magn Reson Med. 2007; 58(5):947–951. [PubMed: 17969117]

Jezzard P, Balaban RS. Correction for geometric distortion in echo planar images from B0 field variations. Magn Reson Med. 1995 Jul; 34(1):65–73. [PubMed: 7674900]

Josephs O, Turner R, Friston K. Event-related fMRI. Hum Brain Mapp. 1997; 5:243–248. [PubMed: 20408223]

Krüger G, Glover GH. Physiological noise in oxygenation-sensitive magnetic resonance imaging. Magn Reson Med. 2001 Oct; 46(4):631–7. [PubMed: 11590638]

Lin FH, Wald LL, Ahlfors SP, Hämäläinen MS, Kwong KK, Belliveau JW. Dynamic magnetic resonance inverse imaging of human brain function. Magn Reson Med. 2006 Oct; 56(4):787–802. [PubMed: 16964616]

Lin FH, Witzel T, Mandeville JB, Polimeni JR, Zeffiro TA, Greve DN, Wiggins G, Wald LL, Belliveau JW. Event-related single-shot volumetric functional magnetic resonance inverse imaging of visual processing. Neuroimage. 2008 Aug 1; 42(1):230–47. Epub 2008 Apr 23. [PubMed: 18538587]

Lin FH, Witzel T, Chang WT, Wen-Kai Tsai K, Wang YH, Kuo WJ, Belliveau JW. K-space reconstruction of magnetic resonance inverse imaging (K-InI) of human visuomotor systems. Neuroimage. 2010 Feb 15; 49(4):3086–98. Epub 2009 Nov 13. [PubMed: 19914383]

Lin FH, Nummenmaa A, Witzel T, Polimeni JR, Zeffiro TA, Wang FN, Belliveau JW. Physiological noise reduction using volumetric functional magnetic resonance inverse imaging. Hum Brain Mapp. 2011 Sep 23. [Epub ahead of print] PMID: 21954026. 10.1002/hbm.21403

Lindquist MA, Zhang CH, Glover G, Shepp L. Rapid three-dimensional functional magnetic resonance imaging of the initial negative BOLD response. J Magn Reson. 2008 Mar; 191(1):100–11. Epub 2008 Jan 3. [PubMed: 18207441]

Mansfield P, Maudsley AA. Planar spin imaging by NMR. J Phys C: Solid State Phys. 1976; 9:L409–L412.

Mansfield P, Harvey PR, Stehling MK. Echo-volumar imaging. MAGMA. 1994; 2:291–294.

Mansfield P, Howseman R, Ordidge R. Volumnar imaging using NMR spin echoes: echo-volumnar imaging EVI at 0.1T. J Phys E. 1977; 22:324–330.

Mathiak K, Posse S. Evaluation of Motion and Realignment for Functional Magnetic Resonance Imaging in Realtime. Magnetic Resonance in Medicine. 2001; 45(1):167–171. [PubMed: 11146500]

Murphy K, Bodurka J, Bandettini PA. How long to scan? The relationship between fMRI temporal signal to noise ratio and necessary scan duration. Neuroimage. 2007 Jan 15; 34(2):565–74. Epub 2006 Nov 22. [PubMed: 17126038]

Mutihac R, Van Hulle MM. Comparison of PCA and ICA for BSS. Rom Rep Phys. 2004; 56(1):20–32.

Mutihac, R.; Posse, S. Univariate Autoregressive Modeling of Functional Echo-Volumar Magnetic Resonance Imaging Data. Proc. 17th Annual Meeting of the Organization of Human Brain Mapping; 2011; Quebec, Canada. p. Abstract 767

Otazo R, et al. Superresolution Parallel Magnetic Resonance Imaging. Neuroimage. Aug 1; 2009 47(1):220–230. [PubMed: 19341804]

Poser BA, Koopmans PJ, Witzel T, Wald LL, Barth M. Three dimensional echo-planar imaging at 7 Tesla. Neuroimage. 2010 May 15; 51(1):261–6. Epub 2010 Feb 6. [PubMed: 20139009]

Posse S, Wiese S, Gembris D, Mathiak K, Kessler C, Grosse-Ruyken M-L, Elghawagh B, Richards T, Dager SR, Kiselev VG. Enhancement of BOLD-Contrast Sensitivity by Single-Shot Multi-Echo Functional MR Imaging. Magnetic Resonance Med. 1999; 42(1):87–97.

Posse S, et al. A New Approach to Measure Single Event Related Brain Activity using Real-Time fMRI: Feasibility of sensory, motor, and higher cognitive tasks. Human Brain Mapping. 2001; 12(1):25–41. [PubMed: 11198103]

Qian W, Glover PM, Bowtell RW. Geometric distortion correction in echo volumar imaging. Proc ISMRM. 2009:4632.

Rabrait C, Ciuciu P, Ribés A, Poupon C, Le Roux P, Dehaine-Lambertz G, Le Bihan D, Lethimonnier F. High temporal resolution functional MRI using parallel echo volumar imaging. J Magn Reson Imaging. 2008 Apr; 27(4):744–53. [PubMed: 18383267]

Raij T, Ahveninen J, Lin FH, Witzel T, Jääskeläinen IP, Letham B, Israeli E, Sahyoun C, Vasios C, Stufflebeam S, Hämäläinen M, Belliveau JW. Onset timing of cross-sensory activations and multisensory interactions in auditory and visual sensory cortices. Eur J Neurosci. 2010 May; 31(10):1772–82. [PubMed: 20584181]

Schöpf V, Windischberger C, Kasess CH, Lanzenberger R, Moser E. Group ICA of resting-state data: a comparison. MAGMA. 2010 Dec; 23(5–6):317–25. Epub 2010 Jun 3. [PubMed: 20521082]

Song AW, Wong EC, Hyde JS. Echo-volume imaging. Magn Reson Med. 1994; 32(5):668–671. [PubMed: 7808270]

Speck O, Hennig J. Functional Imaging by I0- and T2*-Parameter Mapping using Multi-Image-EPI. Magn Reson Med. 1998; 40(2):243–248. [PubMed: 9702706]

Thesen S, Heid O, Mueller E, Schad LR. Prospective acquisition correction for head motion with image-based tracking for real-time fMRI. Magn Reson Med. 2000 Sep; 44(3):457–65. [PubMed: 10975899]

Triantafyllou C, Hoge RD, Krueger G, Wiggins CJ, Potthast A, Wiggins GC, Wald LL. Comparison of physiological noise at 1.5 T, 3 T and 7 T and optimization of fMRI acquisition parameters. Neuroimage. 2005 May 15; 26(1):243–50. [PubMed: 15862224]

van der Zwaag W, Francis S, Bowtell R. Improved echo volumar imaging (EVI) for functional MRI. Magn Reson Med. 2006 Dec; 56(6):1320–7. [PubMed: 17089364]

van der Zwaag W, Kober T, Marques JP, Glover G, Gruetter R, Krueger G. Comparison of single-shot 2D EPI and segmented 3D EVI acquisition for fMRI at 7T. Proc ISMRM. 2009:1550.

Weisskoff RM. Simple measurement of scanner stability for functional NMR imaging of activation in the brain. Magn Reson Med. 1996 Oct; 36(4):643–5. [PubMed: 8892220]

Wiggins, GC.; Alagappan, V.; Potthast, A.; Schmitt, M.; Wiggins, CJ.; Wald, LL. Design Optimization and SNR Performance of 3T 96 Channel Phased Array Head Coils. Proc. 15h International Society for Magnetic Resonance in Medicine 2007; Berlin, Germany. p. 243

Witzel T, Polimeni JR, Wiggins GC, Lin F, Biber S, Hamm M, Seethamraju R, Wald LL. Single-Shot Echo-Volumar Imaging Using Highly Parallel Detection. Proc ISMRM. 2008:1387.

Witzel T, Polimeni JR, Lin F, Nummenmaa A, Wald LL. Single-Shot Whole Brain Echo Volume Imaging for Temporally Resolved Physiological Signals in fMRI. Proc ISMRM. 2011:633.

Worsley KJ, Liao CH, Aston J, Petre V, Duncan GH, Morales F, Evans AC. A general statistical analysis for fMRI data. Neuroimage. 2002 Jan; 15(1):1–15. [PubMed: 11771969]

Yang Y, Mattay VS, Weinberger DR, Frank JA, Duyn JH. Localized echo-volume imaging methods for functional MRI. J Magn Reson Imaging. 1997; 7(2):371–375. [PubMed: 9090593]

Zahneisen B, Grotz T, Lee KJ, Ohlendorf S, Reisert M, Zaitsev M, Hennig J. Three-dimensional MR-encephalography: fast volumetric brain imaging using rosette trajectories. Magn Reson Med. 2011 May; 65(5):1260–8. Epub 2011 Feb 3. 10.1002/mrm.22711 [PubMed: 21294154]

Zaitsev M, Hennig J, Speck O. PSF Mapping with Parallel Imaging Techniques with High Accelerations Factors: Fast, Robust and Flexible Method for EPI Distortion Correction. Magn Reson Med. 2004; 52:1156–66. [PubMed: 15508146]

Highlights

- Echo volumar imaging using multi-slab acquisition and parallel imaging to reduce geometrical distortion
- Real-time image reconstruction and real-time fMRI analysis
- Significantly increased t-scores and % signal change in BOLD contrast fMRI
- Sensitive detection of 5 major resting state networks in short scan times

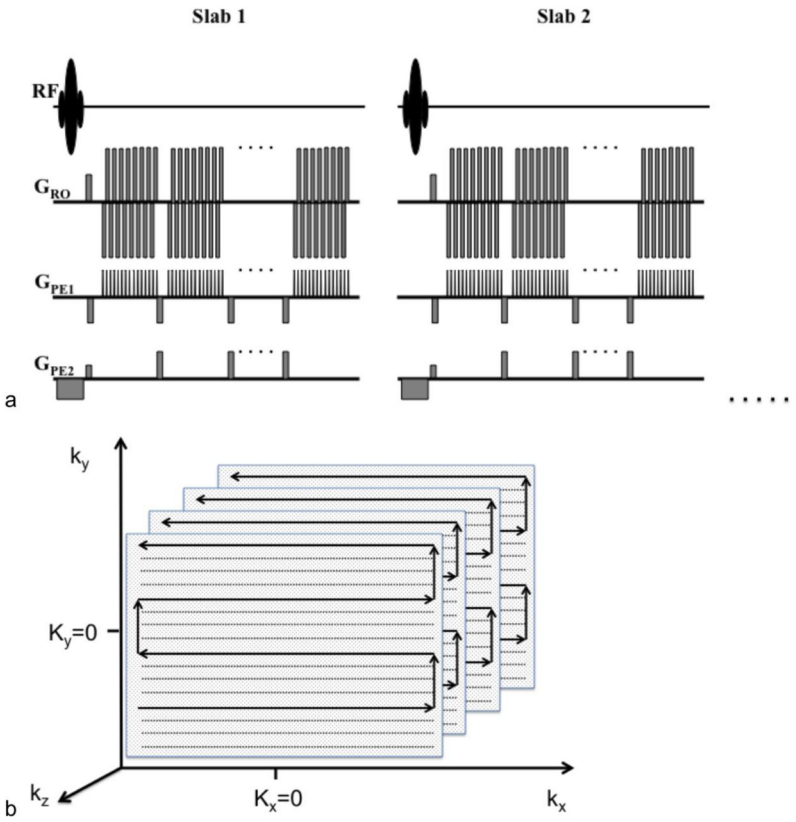

Figure 1.

(a) Schematic diagram of the multi-slab EVI sequence. The pulse sequence for each slab consists of a trapezoidal oscillating readout gradient (G_{RO}) along the readout direction, a blipped primary phase encoding gradient (G_{PE1}) that is rewound at the end of every partition and a blipped secondary phase encoding gradient (G_{PE2}) that encodes the third spatial dimension. (b) K-space trajectory for each slab with 4-fold acceleration in the k_y-direction.

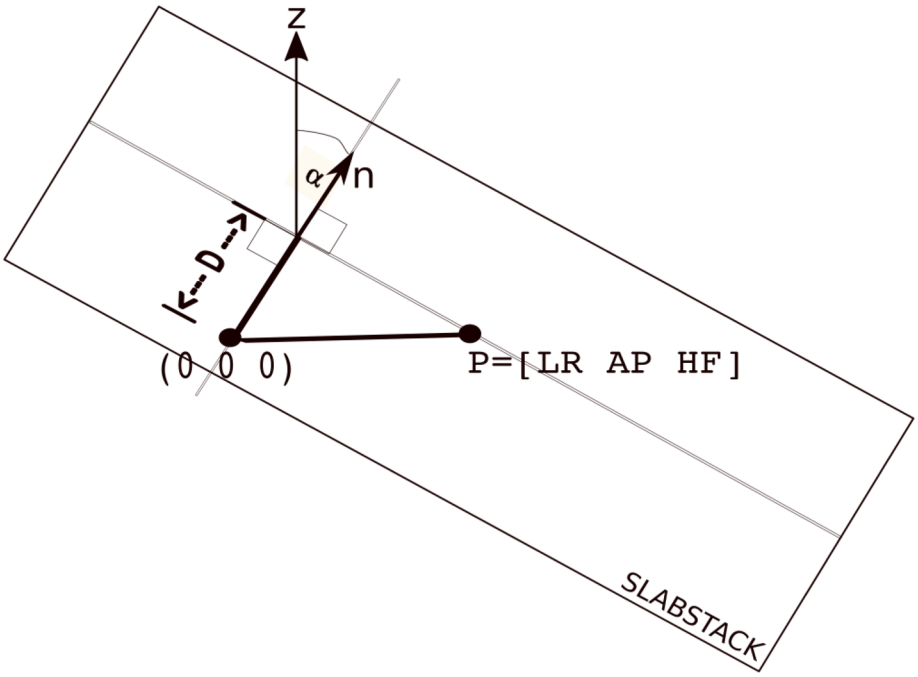

Figure 2.
Geometrical description of the offset computation in Eq.3 in two dimensions. The offset distance D between the slabstack with rotation angle α and the magnet center (0 0 0) corresponds to the projection of the slab position vector $\vec{p}$ with offsets RL, AP, HF onto the normal unit vector of the slabstack ($\vec{n}$).

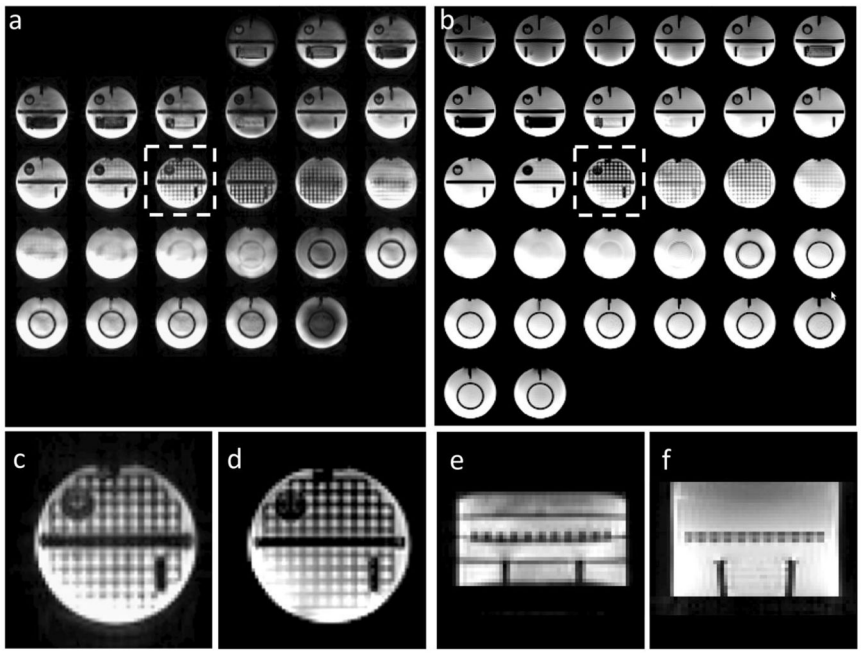

Figure 3.
Comparison of 4-slab EVI (TR: 286 ms) and conventional EPI in a phantom with internal grid structures to assess blurring and distortions. (a) Four-slab EVI raw data. (b) Corresponding EPI raw data. (c) Zoomed multi-slab EVI slice at the inner edge of the 2nd slab from the slice location demarcated by a dashed box in (a). (d) Zoomed EPI slice from the slice location demarcated by a dashed box in (b). (e) Coronal view of multi-slab EVI through the center of (a). The intersection between slabs is visible as 3 dark lines. (f) Coronal view of EPI through the center of (b).

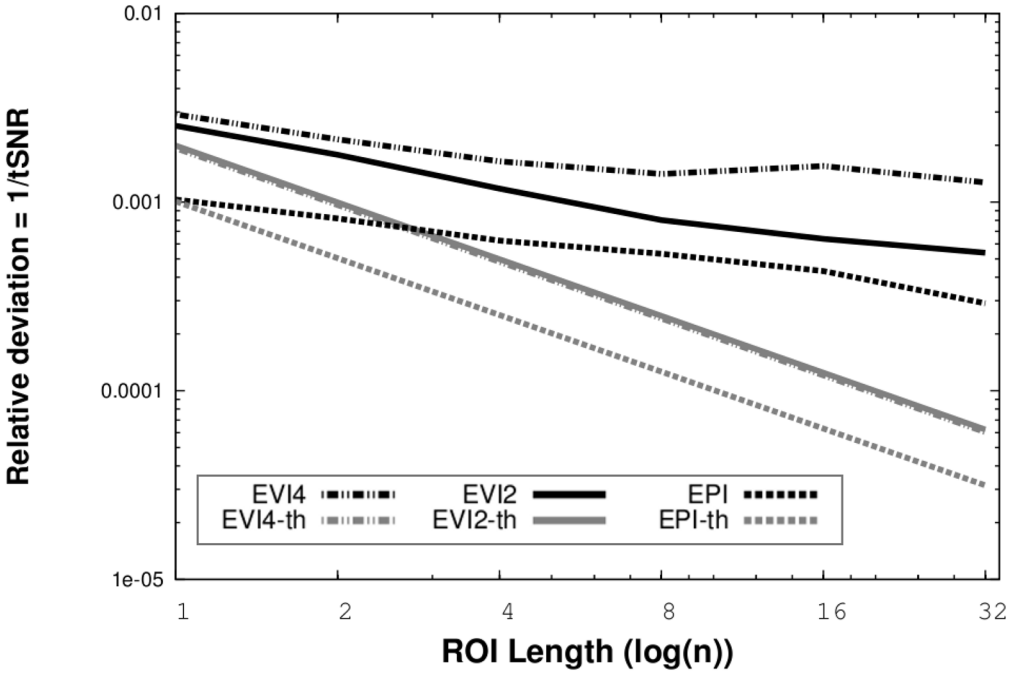

Figure 4.
Relative signal fluctuations measured in multi-slab EVI and conventional EPI data in a cylindrical phantom and the theoretical SNR limits plotted as a function of the ROI length.

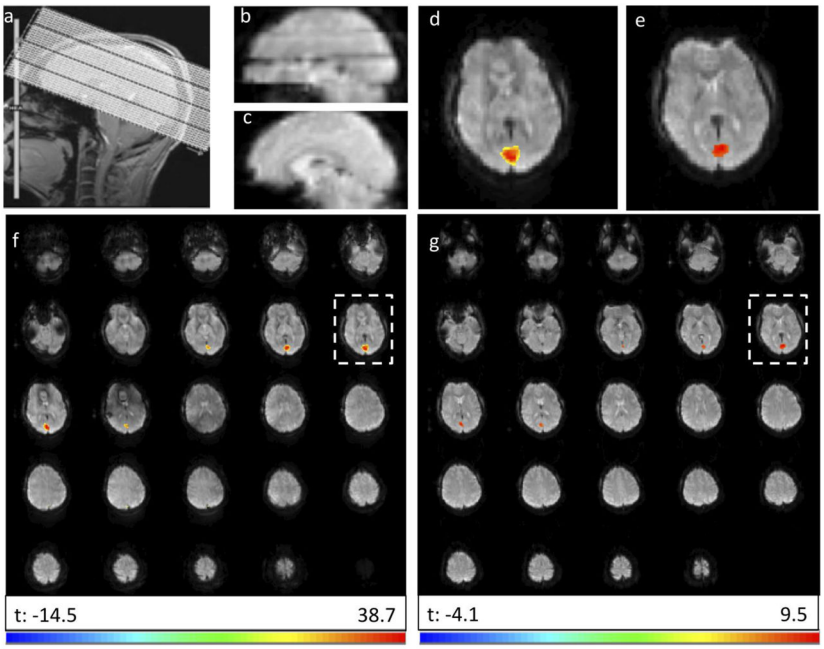

Figure 5.

Comparison of 4-slab EVI (TR: 286 ms) and conventional EPI in vivo. (a) Prescription of slabs in AC/PC orientation. (b) Four-slab EVI raw data in sagittal orientation. The intersection between slabs is visible as 3 dark lines. (c) EPI raw data in sagittal orientation. (d) Zoomed multi-slab EVI slice through visual cortex from the slice location demarcated by a dashed box in (f) with overlaid t-map in visual cortex. (e) Corresponding zoomed EPI slice from the slice location demarcated by a dashed box in (g) with overlaid t-map in visual cortex. (f) Multi-slab EVI with overlaid t-map. (g) Corresponding EPI with overlaid t-map. The EVI t-map was computed with 2 s moving average filter, which matches the temporal resolution of EPI. The t-thresholds were set at the Least Square Mean Estimate of the mean t-scores in visual cortex.

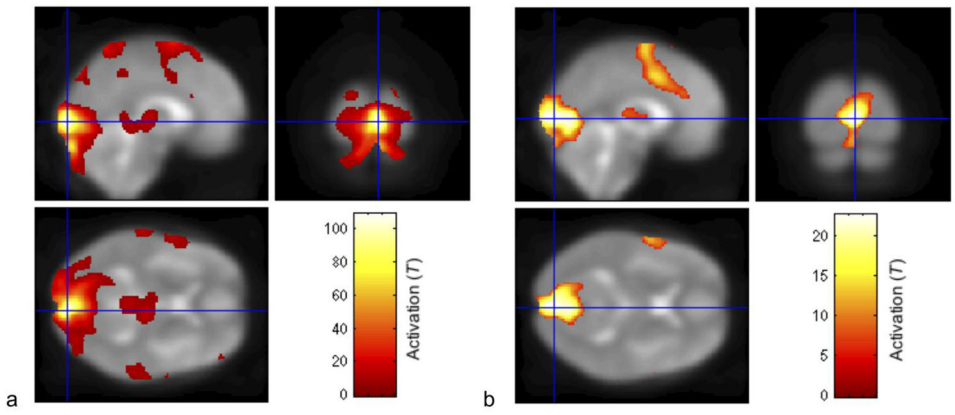

Figure 6.

Single-subject activation maps of a visual-motor task overlaid on the MNI template brain. Data were obtained with (a) 4-slab EVI (TR: 286 ms) and (b) EPI and represent 3 concatenated scans. Activation maps are scaled to maximum t-score, which was considerably larger with 4-slab EVI (108.7) compared to EPI (23.6). Note the larger extent of activation of 4-slab EVI compared to EPI.

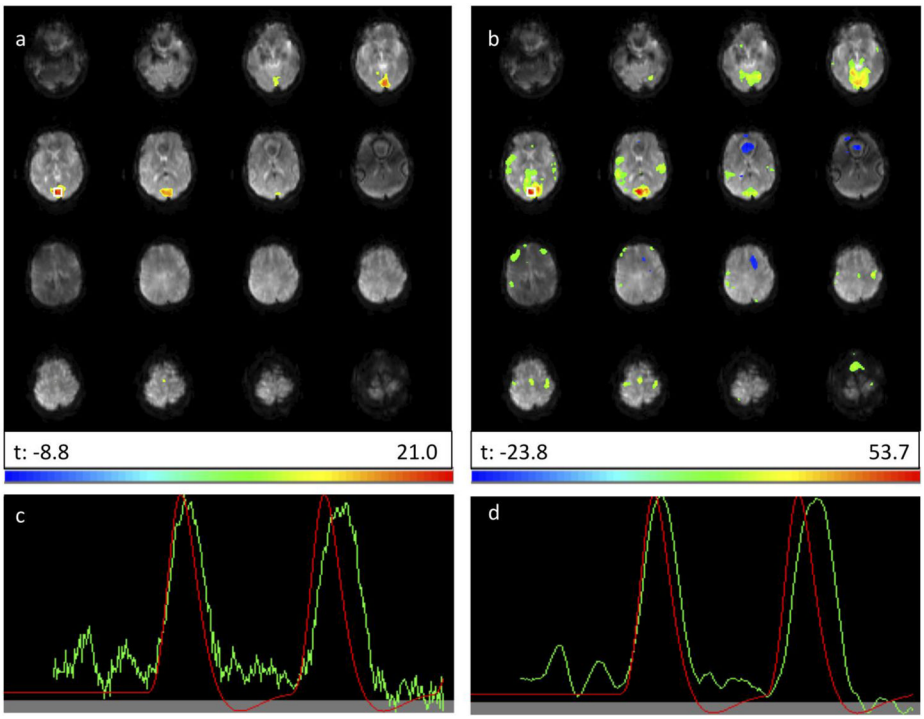

Figure 7.

Real-time fMRI activation map measured during a visual-motor task obtained with 2-slab EVI (TR: 136 ms) without (a,c) and with (b,d) 2 s moving average filter. (a, b) Raw images with overlaid t-map. (b,d) Signal time course from a VOI in visual cortex (Brodmann Areas 17 and 18) marked with a white box in slice 5 (a,b) with overlaid hemodynamic response function model (red) depict task-related signal changes of 11.5 % without moving average filter and 9.7 % with moving average filter. The t-threshold was set at the subjects' mean t-scores in visual cortex.

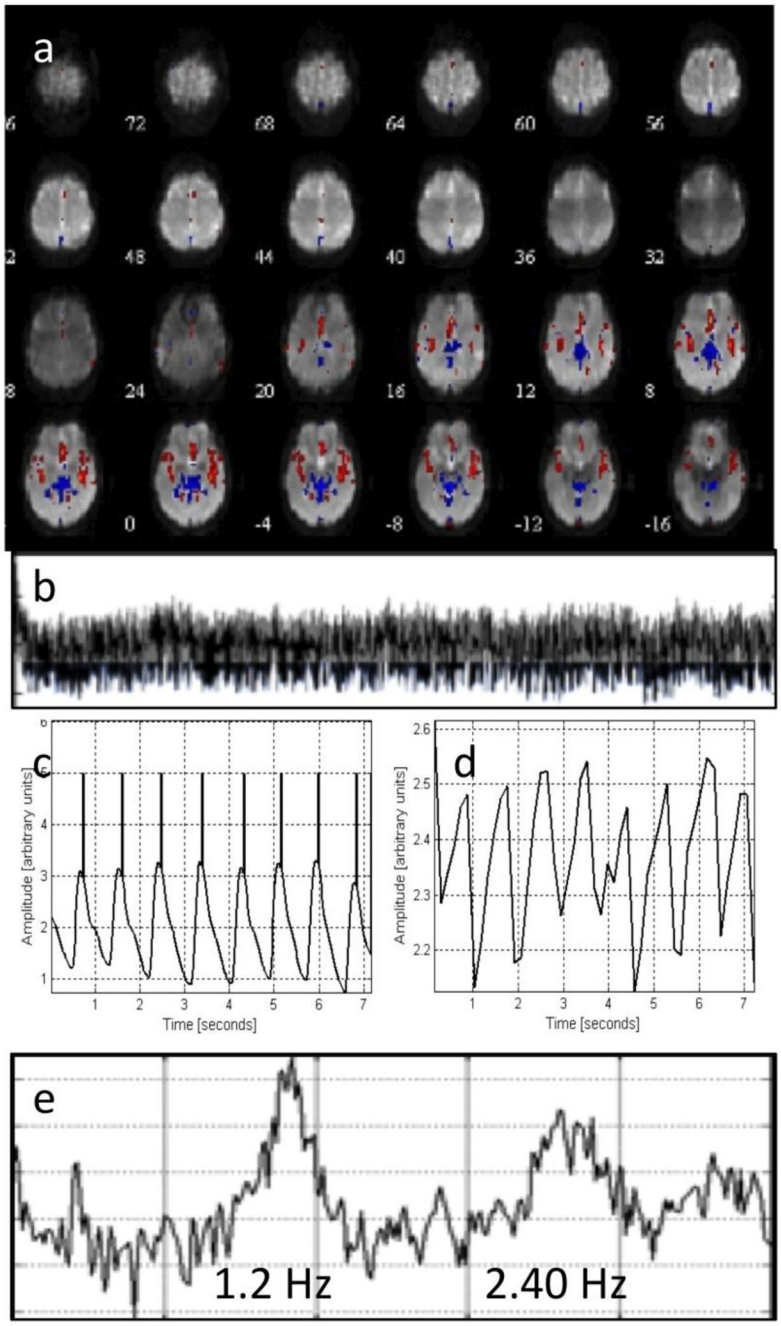

Figure 8.

Physiological noise measured using 2-slab EVI (TR: 135 ms, 108 s scan). (a) An ICA map showing cardiac-related signal changes in brain stem, insular cortex and CSF containing spaces. (b) Corresponding ICA time course. (c) Zoomed section of the peripheral pulse trace and (d) the corresponding cardiac related ICA time course showing signal fluctuation with 850 ms periodicity. (e) Power spectrum of the cardiac-related ICA time course.

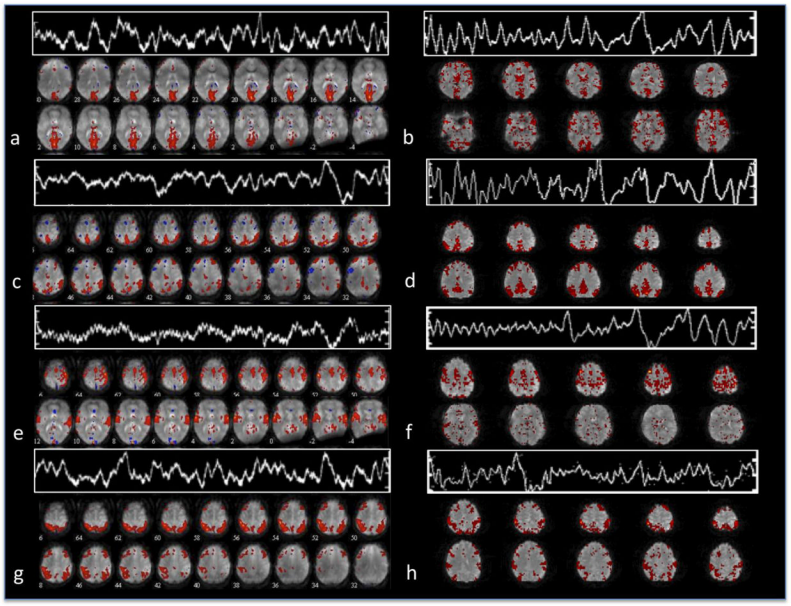

Figure 9.
Major resting state networks with corresponding time courses detected in a single subject using (a,c,e,g) 2-slab EVI with TR: 136 ms and (b,d,f,h) conventional EPI. (a,b) RSN1 (occipital), (c,d) RSN2 (default mode), (e,f) RSN3 (bilateral sensorimotor) + RSN5 (temporal), and (g,h) RSN4 (dorsal parietal and lateral prefrontal).

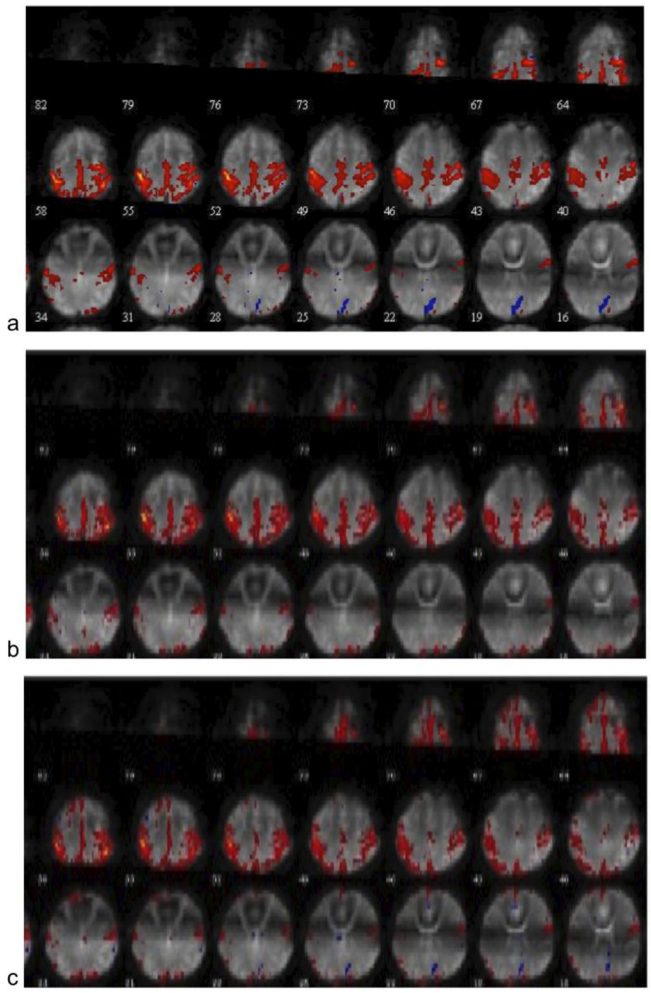

Figure 10.
Sensorimotor resting state networks detected in a single subject using 2-slab EVI (TR: 136 ms) for different scan durations: (a) Full scan (4 min 59 s), (b) simulated scan time of 2 min 30 s and (c) simulated scan time of 75 s.

Table 1

Mean and maximum BOLD signal amplitude (% signal change) in visual and motor cortex for experiment 1 comparing 4-slab EVI (EVI4) with 286 ms temporal resolution, 4-slab EVI with 2 s moving average filter (EVI4-MA) and EPI.

Subject	Scan	VISUAL						MOTOR					
		EVI4		EVI4-MA		EPI		EVI4		EVI4-MA		EPI	
		mean	max	mean	max	mean	max	mean	max	mean	max	mean	max
1	1	4.7%	15.9%	3.4%	10.1 %	2.2%	7.7 %	3.3%	6.2 %	2.0%	4.8 %	1.3%	3.6 %
	2	4.2%	11.5 %	2.8 %	8.8%	2.5%	8.8 %	3.3%	6.7 %	2.0%	5.2 %	1.8%	5.6 %
2	1	4.2%	8.9 %	2.3 %	7.9%	1.8%	6.5 %	3.7%	8.7 %	2.6%	7.6 %	1.2%	4.9 %
3	1	4.9%	13.5 %	3.8 %	13.2 %	3.5%	12.4 %	4.1%	13.7 %	2.5%	12.2 %	1.9%	6.3 %
4	1	4.1%	14.2 %	2.6 %	12.8 %	2.9%	12.1 %	3.8%	5.8 %	2.0%	4.6 %	1.5%	2.6 %
	2	3.8%	13.3 %	2.5 %	12.5 %	2.7%	10.2 %	3.7%	5.3 %	2.1%	3.6 %	1.5%	2.4 %
	3	3.7%	12.5 %	2.5 %	10.6 %	2.6%	12.9 %	3.6%	6.3 %	2.0%	4.0 %	1.6%	3.0 %
Least Squares Mean Estimate		**4.3%**	**12.5 %**	**2.9 %**	**10.5 %**	**2.7%**	**9.7 %**	**3.7%**	**8.5 %**	**2.2%**	**6.9 %**	**1.6%**	**5.1 %**
Standard Error		**0.3%**	**1.2 %**	**0.3 %**	**1.2%**	**0.3%**	**1.2 %**	**0.1%**	**1.5 %**	**0.1%**	**1.5 %**	**0.1%**	**1.5 %**
		EVI4 vs. EPI		**EVI4-MA vs. EPI**		**EVI4-MA vs. EVI4**		**EVI4 vs. EPI**		**EVI4-MA vs. EPI**		**EVI4-MA vs. EVI4**	
		mean	max	mean	max	mean	max	mean	max	mean	max	mean	max
Relative Difference of Least Squares Mean Estimate		**59.3 %**	**28.9 %**	7.4 %	8.2%	**−32.6 %**	−16.0 %	**131.3%**	**66.7 %**	**37.5 %**	**35.3 %**	**−40.5 %**	−18.8 %
Pairwise compariso ns (p-value)[1]		**<0.0001**	**0.0115**	0.3302	0.6339	**<0.0001**	0.0705	**<0.0001**	**0.0002**	**0.0002**	**0.018**	**<0.0001**	0.0683

[1] Scheffé correction for multiple comparisons of least squares means estimates.

Table 2

Mean and maximum t-scores of activation in visual and motor cortex for experiment 1 comparing 4-slab EVI (EVI4) with 286 ms temporal resolution, 4-slab EVI with 2 s moving average filter (EVI4-MA) and EPI.

Subject	Scan	VISUAL						MOTOR					
		EVI4		EVI4-MA		EPI		EVI4		EVI4-MA		EPI	
		mean	max	mean	max	mean	max	mean	max	mean	max	mean	max
1	1	16.7	38.8	27.0	47.0	6.6	9.5	10.6	22.5	15.1	27.8	4.6	7.1
	2	16.0	31.7	26.8	45.3	8.5	11.5	11.1	24.2	16.3	32.0	5.5	8.1
2	1	12.4	33.1	22.3	52.2	6.8	9.8	14.4	35.1	22.5	43.3	6.2	10.2
3	1	19.0	37.1	21.8	43.3	7.2	10.3	9.1	17.7	10.9	23.7	4.2	5.7
4	1	14.0	42.3	20.8	56.6	8.8	12.7	6.2	12.6	10.0	21.5	4.7	6.6
	2	13.9	44.4	21.1	54.7	8.6	13.2	5.8	10.5	9.3	17.8	4.8	6.5
	3	15.0	40.4	21.8	56.0	8.3	11.3	4.7	7.9	7.9	13.4	5.3	7.0
Least Squares Mean Estimate		**15.3**	**37.4**	**23.1**	**49.8**	**7.8**	**10.3**	**9.6**	**20.6**	**13.9**	**27.6**	**5.8**	**9.2**
Standard Error		**0.9**	**1.9**	**0.9**	**1.9**	**0.9**	**1.9**	**1.8**	**4.1**	**1.8**	**4.1**	**1.8**	**4.1**
		EVI4 vs. EPI		**EVI4-MA vs. EPI**		**EVI4-MA vs. EVI4**		**EVI4 vs. EPI**		**EVI4-MA vs. EPI**		**EVI4-MA vs. EVI4**	
		mean	max	mean	max	mean	max	mean	max	mean	max	mean	max
Relative Difference of Least Squares Mean Estimate		**96.2%**	**263.1 %**	**196.2 %**	**383.5 %**	**51.0%**	**33.2%**	**65.5 %**	**123.9 %**	**139.7 %**	**200.0 %**	**44.8 %**	**34.0%**
Pairwise comparison s (p-value)[1]		**<0.0001**	**<0.0001**	**<0.0001**	**<0.0001**	**<0.0001**	**<0.0001**	**0.0208**	**0.0016**	**<0.0001**	**<0.0001**	**0.0097**	**0.0426**

[1] Scheffé correction for multiple comparisons of least squares means estimates.

Table 3

Spatial extents of activation in visual and motor cortex in experiment 1 comparing 4-slab EVI (EVI4) with 286 ms temporal resolution, 4-slab EVI with 2 s moving average filter (EVI4-MA) and EPI.

Subject	Scan	VISUAL			MOTOR		
		EVI4 [voxels]	EVI4-MA [voxels]	EPI [voxels]	EVI4 [voxels]	EVI4-MA [voxels]	EPI [voxels]
1	1	1336	1533	583	652	700	257
	2	1300	1486	1043	598	708	402
2	1	489	910	282	439	461	595
3	1	687	906	277	424	672	147
4	1	989	1276	916	385	594	248
	2	783	1161	994	261	503	370
	3	755	1055	976	178	356	305
Least Squares Mean Estimate		**820.0**	**1104.0**	**639.0**	**431.0**	**582.0**	**343.0**
Standard Error		**164.0**	**164.0**	**164.0**	**63.0**	**63.0**	**63.0**
		EVI4 vs. EPI	**EVI4-MA vs. EPI**	**EVI4-MA vs. EVI4**	**EVI4 vs. EPI**	**EVI4-MA vs. EPI**	**EVI4-MA vs. EVI4**
		[voxels]	[voxels]	[voxels]	[voxels]	[voxels]	[voxels]
Relative Difference of Least Squares Mean Estimate		28.3%	**72.8%**	**34.6%**	25.7%	**69.7%**	35.0%
Pairwise comparison s (p-value)[1]		0.2024	**0.0009**	**0.0318**	0.4581	**0.0115**	0.1203

[1]Scheffé correction for multiple comparisons of least squares means estimates.

Table 4

Temporal signal-to-noise (tSNR) in frontal cortex (BA10 L) for experiment 1 across all non-activated voxels (t<1.0) comparing 4-slab EVI (EVI4) with 286 ms temporal resolution, 4-slab EVI with 2 s moving average filter (EVI4-MA) and EPI.

Subject	Scan	EVI4			EVI4-MA			EPI		
		Extent	tSNR		Extent	tSNR		Extent	tSNR	
		[voxels]	mean	SD	[voxels]	mean	SD	[voxels]	mean	SD
1	1	76	83.1	19.3	53	131.8	44.1	210	175.8	77.1
	2	98	79.0	21.3	54	134.9	55.5	256	137.9	65.0
2	1	55	70.4	22.0	36	99.6	54.3	147	202.6	70.8
3	1	66	79.2	28.4	44	107.2	50.2	197	132.2	69.0
4	1	98	75.1	23.5	64	120.5	51.4	294	157.3	66.4
	2	110	79.2	24.5	70	143.1	59.8	182	168.4	73.2
	3	135	70.0	20.8	106	108.9	45.6	202	144.6	71.5
Least Squares Mean Estimate		**76.6**			**120.9**			**159.8**		
Standard Error		**6.5**			**6.5**			**6.5**		
		EVI4 vs. EPI			**EVI4-MA vs. EPI**			**EVI4-MA vs. EVI4**		
		mean			mean			mean		
Relative Difference of Least Squares Mean Estimate		**−52.1%**			**−24.3%**			**57.8%**		
Pairwise comparison s (p-value)[1]		**<0.0001**			**0.0021**			**0.0006**		

[1]Scheffé correction for multiple comparisons of least squares means estimates.

Table 5

Experiment 2. Comparison of 4-slab EVI (EVI4) with 286 ms temporal resolution and EPI with respect to spatial extent of activation and maximum t-scores. Means and standard errors across multiple scans in 3 subjects (10 EVI4 scans and 7 EPI scans).

		Least-Squares Mean Estimate (SE)		P-Value
Task	**Comparison**	**EVI4**	**EPI**	
Motor	Spatial Extent [Voxels]	21 (5)	9 (6)	0.1264
	T-Scores Max	5.0 (1.5)	2.6 (1.8)	0.3403
Visual	Spatial Extent [Voxels]	149 (16)	10 (19)	**<0.0001**
	T-Scores Max	15.3 (1.3)	5.4 (1.5)	**0.0002**
Auditory	Spatial Extent [Voxels]	69 (7)	11 (8)	**<0.0001**
	T-Scores Max	10.1 (0.8)	3.0 (1.0)	**<0.0001**
Cognitive	Spatial Extent [Voxels]	105 (31)	23 (38)	0.1172
	T-Scores Max	7.7 (1.4)	4.1 (1.7)	0.1279

Table 6

Mean and maximum BOLD signal amplitude (% signal change) in visual and motor cortex for experiment 3 comparing 2-slab EVI with 136 ms temporal resolution and 2-slab EVI with 2 s moving average filter (EVI2 MA).

Subject	Scan	VISUAL				MOTOR			
		EVI2		EVI2-MA		EVI2		EVI2-MA	
		mean	**max**	**mean**	**max**	**mean**	**max**	**mean**	**max**
1	1	2.9%	7.2%	1.3%	6.1%	3.5%	6.0%	1.2%	2.7%
	2	3.3%	9.3%	1.4%	8.0%	3.6%	6.0%	1.3%	3.2%
2	1	4.3%	11.5%	1.8%	10.1%	4.1%	7.1%	1.3%	3.4%
3	1	4.2%	8.2%	1.8%	5.8%	5.1%	9.1%	1.7%	5.0%
	2	3.7%	7.5%	1.4%	5.8%	4.7%	7.2%	1.6%	4.3%
	3	4.3%	8.5%	1.5%	5.9%	4.5%	10.1%	1.5%	5.6%
	4	5.0%	10.4%	1.9%	6.0%	5.2%	10.9%	2.1%	7.9%
Least Squares Mean Estimate		**3.9%**	**9.6%**	**1.6%**	**7.4%**	**4.3%**	**7.6%**	**1.4%**	**4.1%**
Standard Error		**0.3%**	**1.1%**	**0.3%**	**1.1%**	**0.3%**	**1.0%**	**0.3%**	**1.0%**
		EVI2-MA vs. EVI2				**EVI2-MA vs. EVI2**			
		mean	max			mean	max		
Relative Difference of Least Squares Mean Estimate		**−59.0%**	**−22.9%**			**−67.4%**	**−46.1%**		
Pairwise comparisons (p-value)		**<0.0001**	**0.003**			**<0.0001**	**0.0003**		

Table 7

Spatial extents, and mean and maximum t-scores of activation in visual and motor cortex for experiment 3 comparing 2-slab EVI with 136 ms temporal resolution and 2-slab EVI with 2 s moving average filter (EVI2 MA).

Subject	Scan	VISUAL						MOTOR					
		EVI2			EVI2-MA			EVI2			EVI2-MA		
		Extent	t-scores		Extent	t-scores		Extent	t-scores		Extent	t-scores	
		[voxels]	mean	max	[voxels]	mean	max	[voxels]	mean	max	[voxels]	mean	max
1	1	324	9.8	25.8	499	14.2	35.6	120	6.2	15.0	217	11.9	38.2
	2	353	12.3	37.0	482	17.4	54.1	153	6.1	12.8	242	12.7	31.2
2	1	232	9.6	21.0	591	17.6	53.7	124	4.5	8.3	321	11.3	33.2
3	1	162	8.3	19.8	362	11.2	40.5	228	4.8	12.6	475	8.5	25.8
	2	126	9.2	19.1	268	12.1	38.4	220	4.9	12.6	400	9.0	30.4
	3	220	8.8	17.7	220	12.1	34.2	226	5.3	13.9	356	9.1	28.6
	4	331	9.8	23.7	362	14.7	50.5	414	5.8	17.3	342	11.5	38.3
Least Squares Mean Estimate		**280.0**	**10.2**	**23.4**	**428.0**	**14.7**	**43.9**	**188.0**	**5.5**	**13.2**	**312.0**	**10.7**	**32.2**
Standard Error		**60.0**	**1.1**	**2.9**	**60.0**	**1.1**	**2.9**	**51.0**	**0.7**	**1.5**	**51.0**	**0.7**	**1.5**
		EVI2-MA vs. EVI2						EVI2-MA vs. EVI2					
		Extent	t-scores					Extent	t-scores				
		[voxels]	mean	max				[voxels]	mean	max			
Relative Difference of Least Squares Mean Estimate		**52.9 %**	**44.1%**	**87.6 %**				**66.0 %**	**94.5%**	**143.9 %**			
Pairwise comparisons (p-value)		**0.007**	**0.0003**	**0.0003**				**0.005**	**<0.0001**	**<0.0001**			

Table 8

Temporal signal-to-noise (tSNR) in frontal cortex (BA10 L) for experiment 3 across all no-activated voxels (t<1.0) comparing 2-slab EVI (EVI2) with 136 ms temporal resolution and 2-slab EVI with 2 s moving average filter (EVI2 MA).

Subject	Scan	EVI2			EVI2-MA		
		Extent	tSNR		Extent	tSNR	
		[voxels]	mean	SD	[voxels]	mean	SD
1	1	14	70.0	12.1	6	109.1	61.5
	2	9	70.2	23.4	2	179.5	165.2
2	1	74	55.3	11.4	26	117.8	57.8
3	1	31	40.2	18.4	21	69.7	44.5
	2	38	53.1	13.9	19	96.3	45.0
	3	84	46.8	19.7	29	67.9	44.2
	4	49	55.3	15.1	20	58.8	30.3
Least Squares Mean Estimate			**61.8**			**105.9**	
Standard Error			**15.7**			**15.7**	
			EVI2-MA vs. EVI2				
			tSNR				
			mean				
Relative Difference of Least Squares Mean Estimate			**71.4%**				
Pairwise comparisons (p-value)			**<0.0001**				

Table 9

Experiment 4: Maximum Z-scores of resting state networks in four subjects using 2-slab EVI with 136 ms temporal resolution (SD = standard deviation).

	RSN1	RSN2	RSN3	RSN4	RSN5
Subject	**Occipital**	**Default mode network**	**Bilateral sensori-motor**	**Dorsal parietal and lateral prefrontal**	**Temporal and inferior prefrontal**
1	8.8	13.9	9.5	7.9	9.5
2	9.7	9.0	15.2	11.2	15.2
3	17.1	8.9	13.2	15.2	13.2
4	12.0	13.6	9.6	13.3	9.6
Mean	**11.8**	**11.8**	**11.9**	**11.9**	**11.9**
SD	**2.7**	**2.6**	**2.6**	**2.8**	**2.8**